(μ-Oxo)diiron Complexes of Borylated Dimethylglyoximes. Stepwise Ligation to Allosterically Linked Binding Sites and ^{1}H NMR Spectra of Paramagnetic Nitrile, Amine, Imidazole, and Pyridine Derivatives

Isak Vernik and Dennis V. Stynes*

Department of Chemistry, York University, North York, Ontario, Canada M3J 1P3

Received June 29, 1995[⊗]

(μ-Oxo)diiron complexes of [Fe((DMG)BPh$_2$)$_2$]$_2$O (**1**) bind one or two axial ligands within cyclophane-like cavities which lie trans to the oxo bridge. Nonbonded interactions between the bound ligand and the BPh$_2$ superstructure are elucidated. Hindered ligands at one site significantly reduce ligation at the remote site via peripheral contacts operating between the two superstructures surrounding the binding sites. Ligated species are characterized on the basis of visible spectra and paramagnetic shifts in the ^{1}H NMR spectra. The BPh$_2$ phenyl proton shifts were fit to a simple dipolar model. The DMG methyl, imidazole, and pyridine ligand ^{1}H resonances experience contact shifts which differ in magnitude and sign for the various ligated forms, LFe−O−Fe, LFe−O−FeL, and LFe−O−Fe(CH$_3$CN). Contact shifts are consistent with spin transfer from a single unpaired electron on each low-spin iron to π orbitals of the ligands. Restricted rotation of bound ligands within the cyclophane-like cavities is evident.

Introduction

We recently[1] described the new (μ-oxo)diiron complexes [Fe-((DMG)BPh$_2$)$_2$]$_2$O (**1**) and [Fe((DMG)BF$_2$)$_2$]$_2$O (**2**). These species are unique among the large number of (μ-oxo)diiron complexes known[2] in being low spin and existing in both ligated and unligated forms. Only the iron phthalocyanines share these characteristics, and they are not extensively characterized in solution.[3] Heme[4] and iron Schiff base[5] μ-oxo systems ([FeTPP]$_2$O and [Fe(salen)]$_2$O) are high spin and show no tendency to bind ligands trans to the oxo bridge.

X-ray structures in the BPh$_2$ system[1a] reveal a 0.3 Å movement of the irons into the N$_4$ planes and significant rearrangement of the BPh$_2$ superstructure[1a] on ligation. The cyclophane-like cavities surrounding the two binding sites are collapsed in the unligated complex [Fe((DMG)BPh$_2$)$_2$]$_2$O (**1**) and open up in the bis(butylamine) derivative. These structural changes provide a simple mechanism by which binding at one site may be communicated via peripheral contacts to a remote site. The structural changes bear a resemblance to those which occur in the vicinity of the active site in hemoglobin[6] and which are thought to trigger the more extensive conformational changes giving rise to the allosteric effects in Hb.

In this work, we explore the binding of a variety of ligands trans to the oxo bridge in [Fe((DMG)BPh$_2$)$_2$]$_2$O. A negative cooperativity for bulky ligands is documented which is linked to the structural effects described above. In addition, we report the first study of paramagnetic shifts in the ^{1}H NMR spectra of ligated (μ-oxo)diiron complexes.

Experimental Section

The μ-oxo complexes **1** and **2** were obtained as described previously.[1] ^{1}H NMR spectra were recorded on a Bruker ARX 400 MHz spectrometer in CDCl$_3$ or CD$_3$CN with shifts referenced to TMS. NMR titrations were carried out by addition of 5−100 μL of stock ligand solutions in CDCl$_3$ to 0.5 mL of a solution of [Fe((DMG)BPh$_2$)$_2$]$_2$O in the NMR tube. Concentrations of Fe$_2$O were typically 1 mM. Assignments for the BuNH$_2$ protons in Fe((DMG)BPh$_2$)$_2$(PMePh$_2$)-(BuNH$_2$) and for the phenyl protons in [(H$_2$O)Fe((DMG)BPh$_2$)$_2$]$_2$O were verified by COSY experiments.

Spectrophotometric Titrations. Solutions of **1** (5 × 10^{-5} M) in dry CH$_2$Cl$_2$ were titrated with ligands in 1 cm cuvettes (10 cm; 5 × 10^{-6} M **1** for $K > 10^4$) by standard methods.[5a] Where distinctive absorbance changes for each step are observed, spectra were analyzed to give the two equilibrium constants K_1 and K_2. For nitriles and water, the two equilibria are significantly overlapped, preventing (in the absence of values for the extinction coefficients for the intermediate species) a reliable determination of both K's. Application of a Hill equation approximation to the data gives good linear plots of log[($A−A_0$)/($A_{inf}−A$)] vs log [L] at both 407 and 680 nm with slopes in the range 1.1−1.2 for the BPh$_2$ cases and as high as 1.5 in the BF$_2$ system. The tabulated values for K_2 are based on analysis in the 670−720 nm region at the λ_{max} of the fully ligated complex.

In cases where rapid reduction to Fe(II) is observed (primarily for BF$_2$ complexes), absorbance readings were made within seconds of ligand addition using a fresh aliquot of the Fe$_2$O stock solution for each measurement. Reduction is readily apparent on the basis of the distinctive visible spectral features of the Fe^{II}((DMG)BR$_2$)$_2$L$_2$ complexes.[7]

Results

The μ-oxo BPh$_2$ complexes are more stable toward reduction than their BF$_2$ analogues, and the phenyl groups prove advantageous for other reasons as well. In the μ-oxo complexes, the axial phenyl groups are constrained to the distal face (trans to

⊗ Abstract published in *Advance ACS Abstracts,* March 1, 1996.

(1) (a) Vernik, I.; Stynes, *Inorg. Chem.* **1996,** *35,* 2006−2010. (b) Thompson, D. W.; Noglik, H.; Stynes, D. V. *Inorg. Chem.* **1991,** *30,* 4567−4571. (c) Noglik, H.; Thompson, D. W.; Stynes, D. V. *Inorg. Chem.* **1991,** *30,* 4571−4575.

(2) Kurtz, D. M. *Chem. Rev.* **1990,** *90,* 585−606.

(3) (a) Ercolani, C.; Gardini. M.; Murray, K. S.; Pennesi, G.; Rossi, G.; Zwack, P. R. *Inorg. Chem.* **1987,** *26,* 3539−3543. (b) Ercolani, C.; Monacelli, F.; Dzunga, S.; Goedken, V. L.; Pennesi, G.; Rossi, G. *J. Chem. Soc., Dalton Trans.* **1991,** 1309.

(4) La Mar, G. N.; Eaton, G. R.; Holm, R. H.; Walker, F. A. *J. Am. Chem. Soc.* **1973,** *95,* 63−75.

(5) Mukherjee, R. N.; Stack, T. D.; Holm, R. H. *J. Am. Chem. Soc.* **1988,** *110,* 1850−1861.

(6) (a) Baldwin, J.; Chothia, C. *J. Mol. Biol.* **1979,** *129,* 175. (b) Perutz, M. F.; *Annu. Rev. Biochem.* **1979,** *48,* 327.

(7) (a) Stynes, D. V. *Inorg. Chem.* **1994,** *33,* 5022−5029. (b) de Silva, D. G. A. H; Leznoff, D. B.; Impey, G. A.; Vernik, I; Jin, Z.; Stynes, D. V. *Inorg. Chem.* **1995,** *34,* 4015−4025. (c) Thompson, D. W.; Stynes, D. V. *Inorg. Chem.* **1990,** *29,* 3815−3822. (d) Vernik, I.; Stynes, D. V. To be submitted.
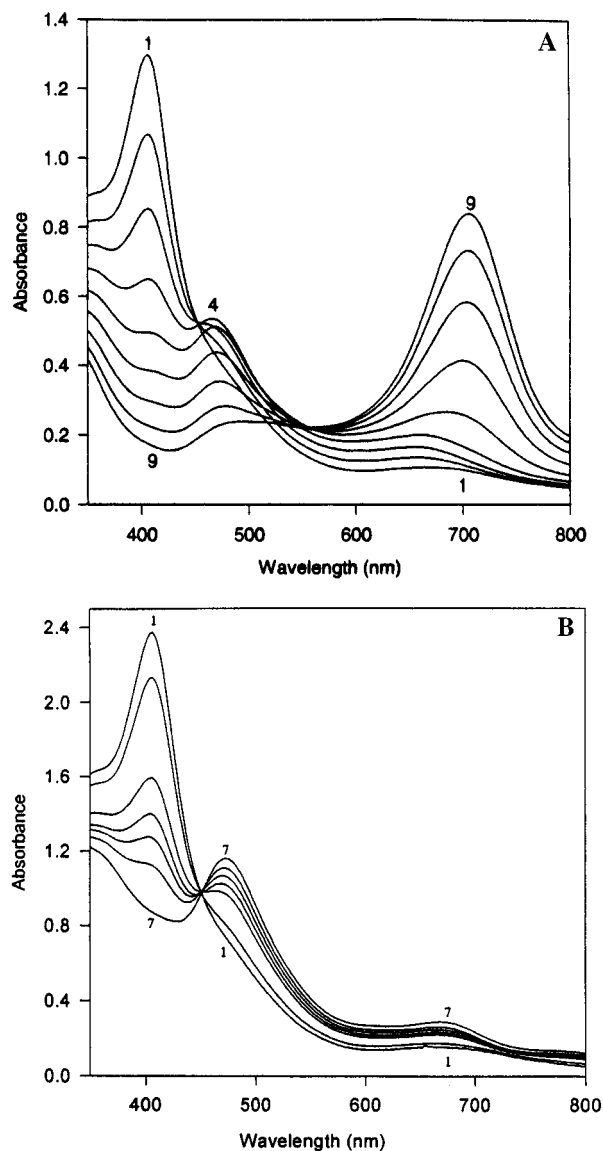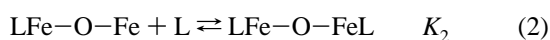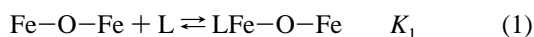
Figure 1. (A) Spectral changes on titration of 0.07 mM **1** with BuNH$_2$ in CH$_2$Cl$_2$. Added [BuNH$_2$] = 0.017, 0.034, 0.05, 0.067, 0.083, 0.10, 0.12, and 2.4 mM in 2−9, respectively. (B) Titration of 0.13 mM **1** with 1,2-Me$_2$Im. Added [1,2-Me$_2$IM] = 0.03, 0.09, 0.12, 0.16, 0.23, and 18 mM in 2−7, respectively.

Table 1. Visible Spectral Data[a] Recorded in CH$_2$Cl$_2$

	BPh$_2$		BF$_2$	
complex	λ_{max}, nm	log ϵ	λ_{max}, nm	log ϵ
[Fe]$_2$O	407	4.27	392	4.29
[Fe(1,2-Me$_2$IM)]−O−[Fe]	475	3.95		
[Fe(4-Me$_2$N(PY))]−O−[Fe][b]	471	3.9		
[Fe(CH$_3$CN)]$_2$O	687	4.01	672	4.03
[Fe(NPT)]$_2$O	693	4.09		
[Fe(TCNE)]$_2$O	600			
[Fe(PY)]$_2$O	728		708	4.06
[Fe(4-Me$_2$N(PY))]$_2$O[b]	723	4.02	707	4.09
[Fe(1-MeIM)]$_2$O	703	4.03	688	4.06
[Fe(BuNH$_2$)]$_2$O	706	4.08	689	4.02
[Fe(H$_2$O)]$_2$O	672	4.02		

[a] Ligated species are generated in situ. [b] An additional band tentatively assigned to a 4-Me$_2$N(PY) to Fe charge transfer is found for 4-Me$_2$N(PY) complexes at 540 nm (BPh$_2$) and 470 nm (BF$_2$).

Table 2. Equilibrium Constants[a] for Ligation to **1** in CH$_2$Cl$_2$

L	log K_1	log K_2	BF$_2$[b,c]
C$_6$H$_5$CN	b	0.3	
CH$_3$CN	b	1.60	2.3
NPT	b	2.3	<1
TCNE	b	3.7	<1
PY	3.8	−0.7	>5
4-Me$_2$N(PY)	>4.5	1.7	>5
1-MeIM	>4.5	3.8	>5
1,2-Me$_2$IM	>4.5	<0	>3.6
i-PrNH$_2$	3.7	1.1	>5
piperidine	>4	1	>5
(+)-PhCH(NH$_2$)Me	1.6	0.8	>5
PhCH$_2$NHCH$_3$	3.3	2.4	>4
PhCH$_2$NH$_2$	>4.5	>4	>5
BuNH$_2$	>6	>5	>5

[a] Estimated error is 0.1 in log K. [b] Overlapped equilibria; only log $K_2 = -\log [L_{1/2}]$ based on analysis at 680 nm is given. [c] Data are for log K_2 in the BF$_2$ system. Lower limits are estimated on the basis of the minimum [L] needed to give >90% bisligation.

etc.) produces spectral changes consistent with the binding of one or two ligands. An intermediate spectrum with a band at 475 nm is assigned to the monoligated species, LFe−O−Fe, while the bisligated complexes, LFe−O−FeL, as reported previously for the BF$_2$ system, have their maximum near 700 nm. For L = nitriles or H$_2$O the two ligation steps overlap with only slight evidence for the middle species. In the case of 1,2-Me$_2$IM (Figure 1B) or pyridine ligands, K_2 is significantly reduced and a clean titration of K_1 is seen.

Clear spectral evidence for a monoligated species is only obtained in the BPh$_2$ system. Assignments based on the visible spectral features are corroborated by the NMR data to follow. The greatest differentiation in K_1 and K_2 was found for the more sterically demanding ligands *i*-PrNH$_2$, 1,2-Me$_2$IM, and pyridines. The visible spectral data for the two systems are summarized in Table 1, and equilibrium constants are collected in Table 2.

NMR Spectra. The ^{1}H NMR spectrum of **1** given in Figure 2A shows sharp resonances between 0 and 10 ppm remarkably similar to those of diamagnetic Fe(II) complexes[7] and consistent with diamagnetism established by the Evans method.[1a] Ligated species were generated by titration, which produces modest shifts and some broadening of the phenyl resonances and much larger effects for ^{1}H resonances assigned to the DMG methyls and axial ligands (Figure 2B,C). The strong BuNH$_2$ and imidazole ligands produce spectra in the slow-ligand-exchange limit. Weaker ligands including nitriles, water, and pyrazines produce averaged resonances consistent with more rapid ligand exchange. As a rough rule of thumb, those with log K's >5 in Table 2 are expected to undergo dissociative ligand exchange at $k < 10^3$ s^{-1}, putting ligand resonances in the slow-exchange limit (400 MHz, for shifts >2 ppm), while those with log K's

the oxo group), where they provide a cyclophane-like binding environment. This feature produces significant differences in the ligation properties of the BPh$_2$ and BF$_2$ complexes.[7]

Ligation. Studies of ligation to **1** were undertaken to probe the energetic consequences of nonbonded interactions with the BPh$_2$ superstructure. The 4-nitrophthalonitrile (NPT) and tetracyanoethylene (TCNE) ligands were selected on the basis of our previous finding of dramatic binding enhancements which can be attributed to Coulombic attractive interactions with the axial phenyls in Fe^{II} derivatives.[7a] A range of amines, imidazoles, and pyridines with varying steric demands were also examined to explore repulsive and other effects.

Typical visible spectra obtained on titration of **1** with L = butylamine in CH$_2$Cl$_2$ are shown in Figure 1A. Two distinct steps are observed consistent with the equilibria:

$$\text{Fe−O−Fe} + \text{L} \rightleftharpoons \text{LFe−O−Fe} \qquad K_1 \qquad (1)$$

$$\text{LFe−O−Fe} + \text{L} \rightleftharpoons \text{LFe−O−FeL} \qquad K_2 \qquad (2)$$

The unligated dimer, **1**, has a visible maximum at 407 nm in dry CH$_2$Cl$_2$. Subsequent addition of ligands (amines, nitriles,

Table 3. Phenyl and DMG Methyl ^{1}H NMR Shifts in Fe((DMG)BPh$_2$)$_2$ Complexes^{a,b}

	eq-Ph			ax-Ph			
L	ortho	meta	para	ortho	meta	para	DMG CH$_3$
			[Fe]$_2$O				
	7.53	7.28	7.22	6.55	6.73	6.75	2.73
			LFeOFe				
BuNH$_2$	8.24	7.91	7.44	5.92	5.74	3.44	−7.92
1-MeIM	8.18	7.90	c	6.07	5.08	3.42	−6.66, −7.67
5-MeIM	8.19	7.91	c	6.08	5.10	3.38	−6.70, −7.78
1,2-Me$_2$IM	8.19	7.77	c	6.12	5.51	3.38	−6.82, −7.37
4-Me$_2$N(PY)	8.2	7.85	7.58	6.03	5.12	3.37	−7.21
2,6-Me$_2$Pz^d	7.98	7.60	7.36	5.60	5.98	4.89	
			LFeOFeL				
BuNH$_2$	8.04	7.67	7.49	7.35	6.46	6.29	−4.16
TCNE	8.08	7.77	7.40	7.30	6.16	6.07	−1.43
NPT	8.05	7.71	7.46	7.28	5.74	5.1	−1.3
CH$_3$CN^e	8.01	7.64	7.38	6.81	6.35	5.83	c
CH$_3$CN^f	8.12	7.74	7.5	7.37	6.43	6.23	−1.71
H$_2$O^g	8.21	7.75	7.47	6.92	6.11	5.81	2.47
H$_2$O^h	8.87	8.25	7.80	6.98	5.43	5.04	−1.16
			Fe^{II}(PY)L^i				
TCNE	7.55	7.28	7.2	7.28	7.08	7.06	2.62
NPT	7.63	7.33	7.14	7.25	6.54	5.75	2.71
CH$_3$CN	7.65	7.35	7.2	7.24	7.0	7.0	2.69

^{a} δ, ppm; in CDCl$_3$ at 300 K except as noted. ^{b} Downfield shifts are positive. ^{c} Not identified. ^{d} Phenyl resonances are an average of ligated and unligated halves of the dimer. ^{e} Not fully ligated in CDCl$_3$ at [CH$_3$CN] = 0.2 M. ^{f} In neat CD$_3$CN. ^{g} At 300 K in H$_2$O-saturated CDCl$_3$. ^{h} Obtained at 233 K in wet CDCl$_3$. ^{i} Data for Fe^{II}((DMG)-BPh$_2$)$_2$(PY)(L) complexes from ref 7a.

Table 4. Observed Axial Ligand ^{1}H NMR Shifts^a at 300 K

L	1	2	3	4	5
		BPh$_2$			
		LFeOFe^b			
1-MeIM	(−2.48)	22.18		14.52	15.72
5-MeIM	11.95	25.98		20.22	(−0.72)
1,2-Me$_2$IM	(−1.87)	(−14.77)		13.61	16.46
4-Me$_2$N(PY)		29.49	12.26	(−6.10)	
		LFeOFeL^b			
1-MeIM	(7.95)				−3.96
1-MeIM^d	(10.19)				−8.73
		BF$_2$			
		LFeOFeA^c			
1-MeIM	(9.82)				−3.4
5-MeIM					(4.04)
1,2-Me$_2$IM	(8.76)	(19.0)			
4-Me$_2$N(PY)		−17.6	−0.49	(14.09)	
4-MePY				(18.8)	
PY		−9.20			
		LFeOFeL^c			
1-MeIM	(9.72)				−2.97
5-MeIM	−3.11	−22		−5.5	(3.80)
1,2-Me$_2$IM	(8.6)	(18.5)			
4-Me$_2$N(PY)		−17	−0.14	(13.75)	
4-MePY				(19.05)	
PY		−21		−9.38	

^{a} δ, ppm. Positive shifts are downfield; values in parentheses are for methyl substituents. ^{b} In CDCl$_3$. ^{c} In CD$_3$CN. ^{d} At 233 K.

<3 will generally be in the fast-exchange limit. Fast exchange produces an averaging of the environments for free and bound ligands as well an averaging of DMG methyl and BPh$_2$ ^{1}H environments among the various ligated μ-oxo forms present in solution.

Some representative NMR spectra are shown in Figures 2, 3, and 5, including examples of fast (Figure 2B) and slow (Figure 2C) exchange, mono (Figure 3A), bis (Figure 3B), and mixed (Figure 5) ligated complexes. The ^{1}H NMR data are summarized in Tables 3−5. Phenyl and DMG methyl shifts in the BPh$_2$ system are given in Table 3. Axial ligand shifts for both BPh$_2$ and BF$_2$ systems are collected in Table 4. The DMG methyl shifts for the various BF$_2$ and BPh$_2$ complexes are compared in Table 5.
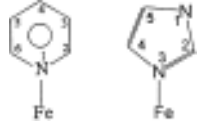
Slow-Exchange Cases. In slow-exchange cases, distinct resonances for each of the three ligated forms are apparent and most of the resonances may be confidently assigned on the basis of their rise and fall vs [L] and of a similar pattern of shifts for a range of different axial ligands.

The mono- and bisligated species show paramagnetic effects manifested most clearly in the appearance of broad DMG methyl resonances upfield of TMS and large upfield or downfield shifts of axial ligand resonances. For the monoligated BuNH$_2$ species, two distinct DMG methyl resonances each integrating to 12 protons are found, one sharper peak at +6.4 ppm associated with the unligated half and a second broader resonance upfield of TMS at −7.9 ppm attributed to the ligated half of the μ-oxo dimer. For the bisligated butylamine complex, a single DMG methyl resonance is found at −4.16 ppm which integrates to all 24 protons.

The β-CH$_2$, γ-CH$_2$, and δ-CH$_3$ ^{1}H resonances for the coordinated BuNH$_2$ were located well upfield of their diamagnetic positions with line widths decreasing with distance from the iron. The α proton resonances are expected to be broad and may lie under the DMG resonance.

A similar pattern is found for 1-MeIM except that a diastereotopic splitting of the DMG methyl resonances occurs

as seen in Figure 3. This splitting is found for all the μ-oxo BPh$_2$ imidazole derivatives but not for μ-oxo BF$_2$ complexes. It is a result of hindered rotation within the cyclophane-like cavity which constrains the N1 side of the imidazole ring to one side of the complex. Only the high-field DMG methyl resonance is split for the monoligated species while four diasterotopic methyl resonances are found for the bis 1-MeIM complex. The spread of the otherwise equivalent methyl resonances for the BPh$_2$ system resembles a similar effect noted for porphyrin methyl substituents in low-spin paramagnetic hemoproteins.[8] Constraints on the imidazole ring orientation are involved in both cases.

Imidazole ring resonances are found at low field (10−30 ppm) for the monoligated complex and high field (above TMS) for the bisligated species. The imidazole CH$_3$ substituent experiences shifts in the direction opposite to those of ring protons in both cases as expected for a π spin delocalization mechanism.[9] Some of the imidazole proton assignments were clarified on the basis of the low-temperature spectrum shown in Figure 3B. The ring 2- and 4-proton resonances were not located for the bis complex but are expected to be broader and may lie much farther upfield or under the DMG resonances. A greater number of assignments were possible for bisligated complexes in the BF$_2$ system.

The hindered 1,2-Me$_2$IM ligand produces only the monoligated species, consistent with the visible spectroscopic results above. 4-Me$_2$NPY is the strongest of the pyridine ligands surveyed and gives a slow-exchange spectrum for the monoligated species. The bis 4-Me$_2$N(PY) complex which forms only at [L] > 0.01 M lies in the fast-exchange limit, and only the DMG methyl resonance was assigned. In both monoligated 1,2-

(8) Traylor, T. G.; Berzinis, A. P. *J. Am. Chem. Soc.* **1980**, *102*, 2844−2846.
(9) Goff, H. M. In *Iron Porphyrins*; Lever, A. B. P., Gray, H. B., Eds.; Addison Wesley: Reading, MA, 1983; Part 1, Chapter 4.
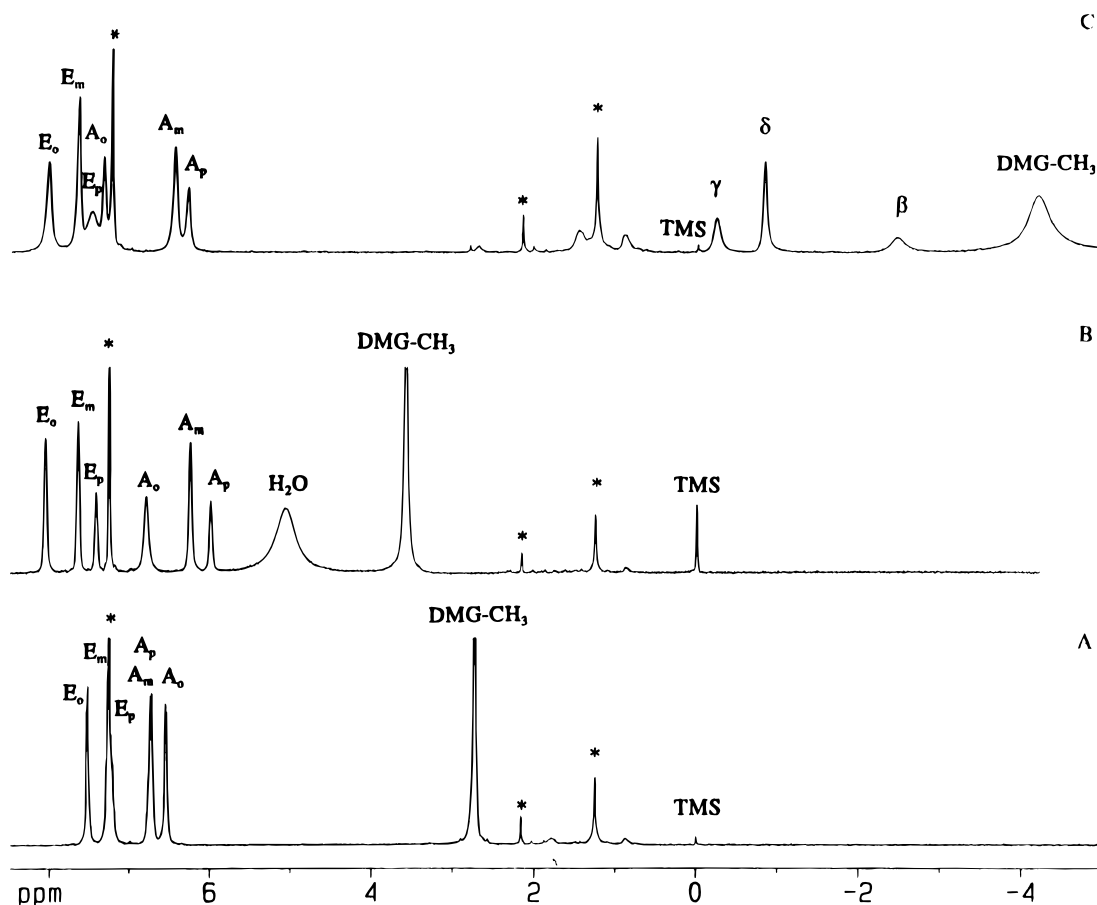
Figure 2. 400 MHz ^{1}H NMR spectra in CDCl$_3$ at 300 K: (A) Fe((DMG)BPh$_2$)]$_2$O; (B) **1** + H$_2$O; (C) **1** + 2.5 equiv of BuNH$_2$. * marks solvent or impurity peaks.

Table 5. DMG Methyl ^{1}H NMR Shifts^a at 300 K

	BPh$_2$			BF$_2$	
L	LFeOFe^b	LFeOFeL^{c,d}	LFeOFeA^{c,d}	LFeOFeL^{c,d}	AFeOFeL^{c,e}
CH$_3$CN		−1.7	−1.7	−4.20	−4.20
BuNH$_2$	−7.92, +6.49	−4.16	−3.19	−6.40	−5.26, −5.62
1-MeIM	−6.66, +6.09	−3.78	−3.88	−6.86	−5.30, −5.94
	−7.67	−4.13	−5.17		
		−6.07			
		−6.41			
5-MeIM	−6.70, +6.09	−4.03		−6.95	−5.40, −5.92
	−7.78	−4.18			
		−6.23			
		−6.38			
1,2-Me$_2$Im	−6.82, +6.12	f	−6.42	−6.2	−4.40, −7.15
	−7.37		−6.85	−6.57	
				−7.68	
				−8.04	
Me$_2$N(PY)	−7.21, +6.04	−5.36	−5.96	−7.37	−4.92, −6.90
4-Me(PY)	f			−6.85	−4.36, −6.84
PY	f			−6.74	−4.22, −6.86

^{a} δ, ppm; in CDCl$_3$ except as noted; positive shifts are downfield from TMS. ^{b} The positive shift is assigned to the DMG methyls on the unligated half. ^{c} In CD$_3$CN. ^{d} Only the resonance assigned to the ligated half is observed. ^{e} The more negative shift is assigned to the ligated half. ^{f} Not observed due to weak binding or rapid exchange.

Me$_2$IM and 4-Me$_2$N(PY) cases, axial ring protons are found downfield and methyl substituents found upfield. Other pyridine ligands typically gave exchange-broadened spectra at room temperature (note K's in Table 2), and no assignments were possible at 300 K. A more extensive data set for pyridine complexes was obtained for the more inert BF$_2$ system as described below.

Fast-Exchange Cases. The nitrile ligands exchange rapidly producing a single set of species-averaged BPh$_2$ resonances for the various μ-oxo complexes which shift with changes in [L] as shown in Figure 4A for L = 4-nitrophthalonitrile (NPT). An

averaging of resonances due to free and coordinated NPT was also observed. The weaker binding and rapid exchange among different ligated forms result in pronounced broadening and early disappearance of the DMG Me resonance of **1** during titrations with these ligands. Only when the bisligated species is fully formed (at high [RCN] or for RCN = TCNE) does the methyl resonance reappear as a broad resonance upfield of TMS. No explicit evidence for the monoligated complex is found in NMR titrations with the nitrile ligands.

The 2,6-Me$_2$PZ ligand produces only the monoligated complex at moderate [L] (based on its visible spectrum) and lies in
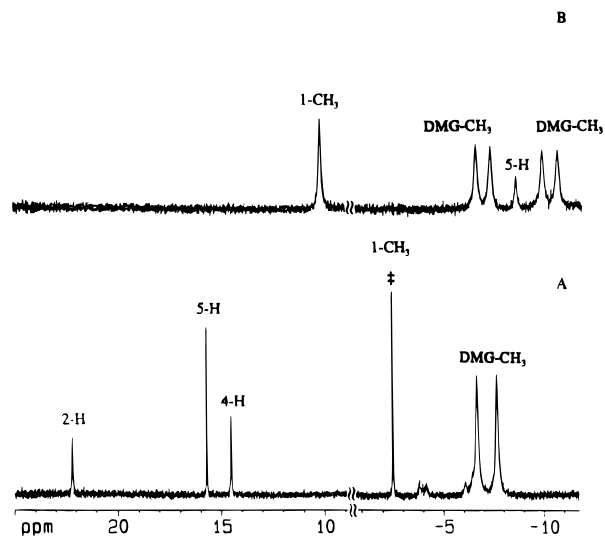
Figure 3. High- and low-field regions in the 400 MHz ^{1}H NMR spectra of MeIM complexes of **1** in CDCl$_3$: (A) mono (**1** + 1 equiv MeIM) at 300 K; (B) bis (**1** + 2 equiv of MeIM) at 233 K. (‡: The sharp 1-CH$_3$ resonance is truncated in part A.)
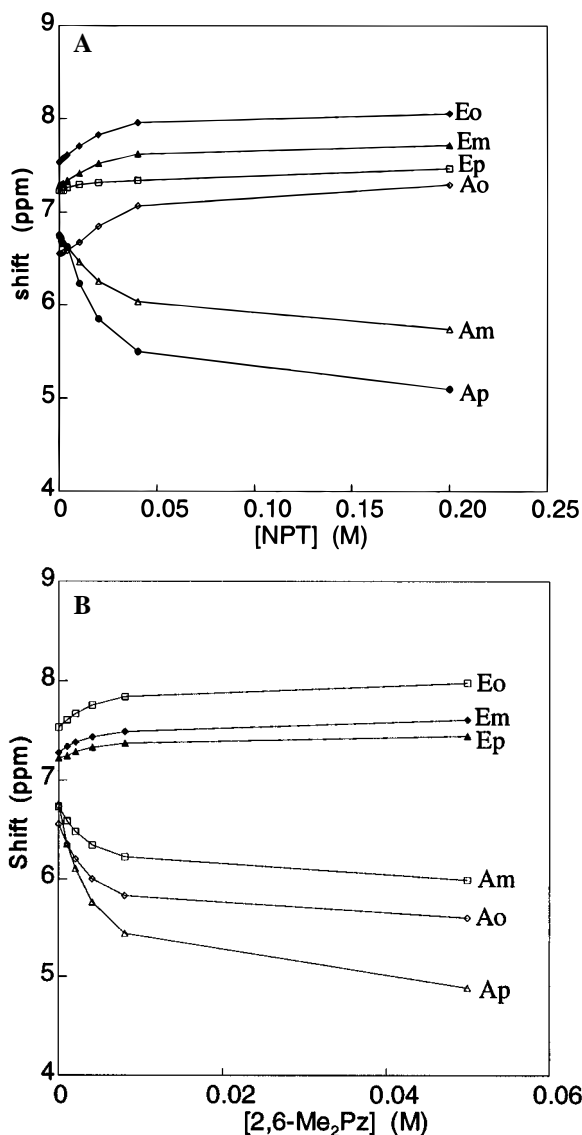

Figure 4. ^{1}H NMR shifts of phenyl resonances during the titration of **1** in CDCl$_3$ at 300 K with weak ligands: (A) L = 4-nitrophthalonitrile (NPT); (B) L = 2,6-Me$_2$PZ.

the fast-exchange limit. The tracking of the phenyl proton resonances in this case shows a different pattern (Figure 4B)
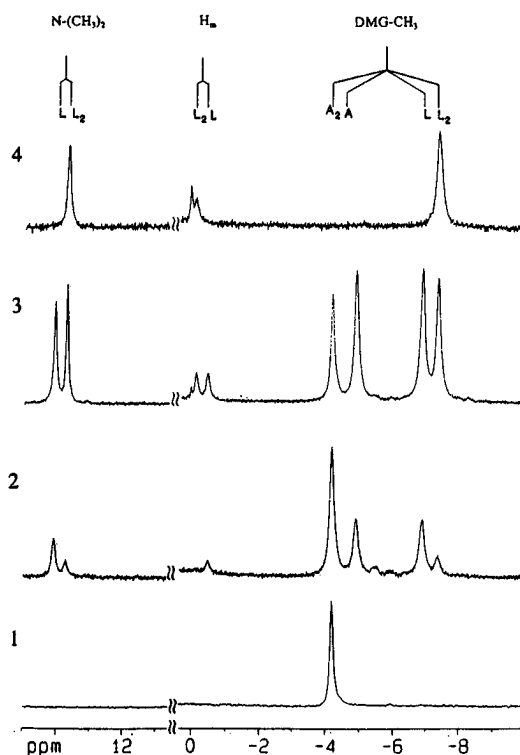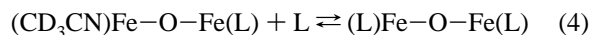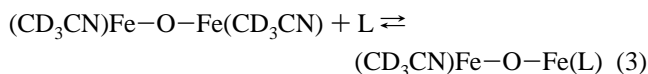

Figure 5. 400 MHz NMR spectra during the titration of (CD$_3$CN)-Fe-O-Fe(CD$_3$CN) (BF$_2$ complex) with 4-Me$_2$N(PY) in CD$_3$CN: 1, (CD$_3$CN)Fe—O—Fe(CD$_3$CN); 4, (4-Me$_2$N(PY))Fe—O—Fe(4-Me$_2$N-(PY)). Spectra 2 and 3 contain data for the mixed-ligated complex (4—Me$_2$N(PY))Fe—O—Fe(CD$_3$CN) in combination with bisligated species.

with the resonance assigned to the ortho axial phenyl protons moving upfield. This feature is consistent with subsequent analysis of the contributions of dipolar effects in monoligated complexes. The axial phenyl shifts for 2,6-Me$_2$PZ are consistent with an average for the collapsed and open cavities in the monoligated complex.

Addition of water causes shifts in the phenyl resonances much like those observed with nitriles (Figure 2B). The DMG methyl peak broadens (but does not disappear as is the case with nitriles) and gradually moves downfield with increasing [H$_2$O], to about 5 ppm. At higher [H$_2$O] it then moves back upfield to 2.5 ppm in water-saturated CDCl$_3$. The initial move downfield is consistent with contributions from a monoligated species, while the subsequent movement upfield is consistent with the diaquo species. Effects similar to those on adding water (both visible and NMR) are produced on lowering the temperature of CDCl$_3$ solutions of **1** and are presumed to also be due to water ligation.

BF$_2$ System. In this system, rapid reduction of the μ-oxo dimers occurs in CDCl$_3$ on adding amine ligands. However, the rate of reduction of the bisligated complexes has a 1/[L] dependence,[1c] making the reduction much slower at high [L] or [CH$_3$CN]. We have therefore obtained NMR spectra for the species shown in eqs 3 and 4 in CD$_3$CN solution. Typical spectral data are shown in Figure 5.

$$(CD_3CN)Fe-O-Fe(CD_3CN) + L \rightleftharpoons$$
$$(CD_3CN)Fe-O-Fe(L) \quad (3)$$

$$(CD_3CN)Fe-O-Fe(L) + L \rightleftharpoons (L)Fe-O-Fe(L) \quad (4)$$

The symmetrically ligated species show isotropic shifts similar to those of their BPh$_2$ analogues. The DMG methyls are all found upfield of TMS. Methyl substituents on imidazoles and pyridine ligands are found well downfield of their diamagnetic positions, while imidazole and pyridine ring protons are shifted

upfield. The greater binding constants, K_2, in the BF_2 system put the pyridine ligands in the slow-exchange limit at 300 K.

The unsymmetrically ligated $(CD_3CN)Fe-O-Fe(L)$ species display distinct DMG methyl and axial ligand resonances with shifts near but not identical to those of the symmetrically ligated species. The shifts do NOT resemble those of the monoligated $Fe-O-Fe(L)$ species observed in the BPh_2 system in $CDCl_3$, and no NMR resonances for a monoligated species could be obtained in the BF_2 system. The splitting of the DMG methyl resonances as a result of hindered rotation of imidazole ligands is evident only in the $1,2-Me_2IM$ case. This contrasts with the BPh_2 system, where hindered rotation is found in all imidazole complexes. The axial fluorines provide a much smaller rotational barrier than the phenyls. Rotation in the $1,2-Me_2IM$ case is restricted by contact between the 2-Me substituent and the axial fluorines. Without a 2-substituent, ligand rotation is fast on the NMR time scale at 300 K.

Mixed-ligated complexes are also obtained in the BPh_2 system in CD_3CN; however the increased steric effects in this system are evident. Those ligands displaying reduced values of K_2 (pyridines and $1,2-Me_2IM$) were reluctant to add CH_3CN to the vacant remote site in $LFe-O-Fe$ and also bind poorly to the $[(CH_3CN)Fe]_2O$ complex. The reduced affinity for CH_3CN in mixed-ligand species of the BPh_2 system is believed to be responsible for our failure to observe the DMG CH_3 resonance associated with the CH_3CN ligated half of the mixed dimer.

Discussion

The equilibrium constants for ligation in the BF_2 and BPh_2 systems are compared in Table 2. In general, the affinity of these systems for ligands is at least 6 orders of magnitude greater than that of heme or Fe(salen) μ-oxo systems, which show no evidence for ligation even in neat pyridine. The binding is however generally weaker than that found in $Fe^{II}((DMG)BR_2)_2$ complexes. Peripheral effects of the BPh_2 groups differ from those in monomeric Fe(II) complexes. While axial phenyls in the monomeric complexes may flip to relieve repulsions with axial ligands, both axial phenyl groups are constrained to the distal face in the μ-oxo complexes.

The trend in the BPh_2 system for the various nitriles, PhCN < CH_3CN < NPT < TCNE, parallels those elucidated previously for Fe(II) derivatives[7a] in which Coulombic attractions between electron-deficient regions of the nitrile ligands and the electron-rich π face of the phenyl groups produce binding enhancements of several orders of magnitude. Except in these cases, the binding to the μ-oxo BPh_2 complexes (in terms of K_2) is weaker than that in the BF_2 system.

The reductions in K_2 in the BPh_2 system for the bulkier ligands are indicative of strong communication between the two binding sites. This communication is believed to occur via close contacts associated with equatorial phenyls on the proximal face evident in the X-ray structural results. These contacts are aggravated by the movement of the iron with respect to the N_4 planes and by effects associated with the opening of the binding cavity surrounding the ligated site. Pyridines, pyrazines, i-PrNH$_2$, and the hindered $1,2-Me_2IM$ show the greatest reductions in K_2. Note that the secondary amine MeBzNH experiences a smaller effect than the branched-chain primary amines. Substituents on the α-carbon have the greatest effect presumably by exerting pressure on the face[10] of the N_4

macrocycle. This face strain may be relieved by a movement of the iron (starting on the oxo side) into or through the N_4 plane.

The magnitude of the effect is unexpectedly large for the pyridine ligands. When pyridine binds inside the cyclophane cavity in Fe(II) complexes, the iron is found displaced toward the pyridine and the cavity.[7d] In the μ-oxo species, the iron is found displaced toward the oxo group and away from the cavity. A greater movement of the iron toward the distal side would tend to aggravate interfacial contacts on the proximal side.

The interactions on the oxo face appear not to play an important role in ligation as long as the unligated iron lies well out of the N_4 plane toward the oxo group, and the distal superstructure is collapsed as found in **1**. Severe repulsions are introduced only on binding a second ligand. The lack of a similar effect in the BF_2 system is strong evidence that the effect is communicated primarily via the peripheral phenyl contacts and not via electronic or other phenomena operating directly through the μ-oxo bridge.

Another indication of communication between the two binding sites may be found in the ligand redistribution equilibrium given in eq 5. A good estimate of the equilibrium

$$2(CH_3CN)Fe-O-Fe(L) \rightleftharpoons$$
$$(CH_3CN)Fe-O-Fe(CH_3CN) + (L)Fe-O-Fe(L) \quad (5)$$
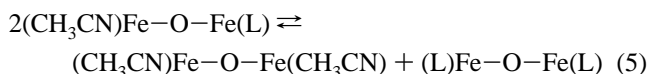
constant for this reaction (K_5) is obtained by integration of the DMG methyl peaks in the NMR. In the BF_2 system values of about 0.2 are obtained (statistical effects would give $K_5 = 0.25$). In the BPh_2 system comparable values are found for unhindered ligands (MeIM, BuNH$_2$), but much reduced values are evident for the hindered ligands, which also show reduced values of K_2 in Table 2.

The magnitude of the negative cooperativity may be estimated on the basis of the K_1/K_2 ratio. For the PY case, we estimate that the second site experiences a reduction in ligation free energy of 6 kcal/mol. This is much larger than the ligation free energy differences between R and T state Hb. It should be noted however that positive cooperativity is relatively rare compared to negative cooperativity, which tends to arise naturally in certain sterically crowded systems.

NMR. This work is the first report of the effect of axial ligation on the NMR spectra of low-spin (μ-oxo)diiron complexes.[11] Heme[4] and Schiff base[5] (μ-oxo)diiron complexes do not bind axial ligands, and their NMR resonances are those of high-spin antiferromagnetically coupled pentacoordinate irons.

Our low-spin μ-oxo complexes have more in common with monomeric low-spin Fe(III) hemes[12] involving imidazole and cyanide ligands. No analogous monomeric $Fe((DMG)BR_2)_2$-IM_2^+ complexes are known, as reduction to Fe(II) is rapid in the bis(dioxime) systems. Studies of the NMR of low-spin hemes have primarily focused on porphyrin ring proton resonances.[8,9] Only at low temperatures is the exchange rate of the imidazole ligands slow enough to permit the detection of imidazole protons in $Fe(porphyrin)(IM)_2^+$ complexes.

As seen above, most imidazole- and several pyridine-ligated complexes of the μ-oxo $Fe((DMG)BR_2)_2$ systems lie in the slow-exchange limit and their NMR spectra reveal the effects of dipolar and contact shifts for axial ligand, DMG methyl, and BPh_2 protons. A model which assumes the dominance of dipolar contributions to the BPh_2 ^1H shifts and predominantly

(10) Contacts between the N_4 plane and ortho hydrogens of pyridines are more severe than those for imidazoles as a consequence of the smaller internal angles in five-membered rings: Scheidt, W. R.; Gouterman, M. In *Iron Porphyrins*; Lever, A. B. P., Gray, H. B., Eds.; Addison Wesley: Reading, MA, 1983; Part 1, pp 91−139.

(11) Some NMR data for μ-oxo iron phenanthroline complexes are described: Meanage, S.; Vincent, J.; Lambeaux, C.; Chottard, G.; Grand, A.; Fontecave, M. *Inorg. Chem.* **1993**, *32*, 4766−4773.

(12) (a) La Mar, G. N.; Walker, F. J. *J. Am. Chem. Soc.* **1973**, *95*, 1781− 1790. (b) Satterlee, J. D.; La Mar, G. N. *J. Am. Chem. Soc.* **1976**, *98*, 2804−2808.

Table 6. Geometric Factors[a] for Dipolar Analysis of Phenyl Proton Resonances

	equatorial			axial			
	o	m	p	o	m	p	DMG CH$_3$
			Mono BuNH$_2$[b]				
r, Å	5.36	7.51	8.38	4.5	5.2	5.4	4.56
θ, deg	91.8	97.4	99.4	50	35	10	90.6
G	−6.5	−2.2	−1.6	3.0	7.0	12.0	−10.5
			Bis BuNH$_2$[c]				
r, Å	5.36	7.51	8.38	4.45	6.15	6.84	4.56
θ, deg	91.8	97.4	99.4	58.8	41.0	32.0	90.6
G	−6.5	−2.2	−1.6	−2.2	3.0	3.6	−10.5

[a] $G = (3(\cos^2 \theta) - 1)/r^3$ ($\times 10^{21}$ cm^3). [b] Analysis is for axial phenyl protons on unligated half and equatorial phenyl protons on ligated half ONLY assuming the collapsed geometry shown in Figure 6B. [c] Structural data from ref 1a.

contact contributions for the axial ligand and DMG methyl resonances provides a satisfactory accounting of the features observed.

Dipolar Analysis. The isotropic shifts for the BPh$_2$ phenyl protons are expected to be predominantly dipolar in origin by analogy with the phenyls of iron tetraphenylporphyrins[12] and on the basis of a pattern of shifts consistent with geometric factors calculated from structural data. We assume axial symmetry and neglect contributions from the remote iron in evaluating the dipolar shifts.[13] Geometric factors for the bisligated BuNH$_2$ complex were calculated from the geometry found in the X-ray structure of this complex.[1a]

No structural data are available for a monoligated species. Therefore a hybrid of the ligated and unligated structures was assumed with a linear Fe−O−Fe bridge and both irons in the N$_4$ planes. Geometric data for both cases are given in Table 6. A somewhat greater collapse of the vacant binding cavity than that found in the unligated dimer was required in order to fit the pattern of shifts found for the monoligated species. Much larger upfield shifts are seen for one set of phenyl proton resonances. These are assigned to axial BPh$_2$ protons around the void. The solution paramagnetism as measured by the Evans method is essentially the same for mono and bis species, and no correspondingly large effect is seen for the equatorial protons.

Plots of the observed shifts vs geometric factors calculated from the structure of **1-(BuNH$_2$)$_2$** and the assumed geometry for **1-BuNH$_2$** are given in Figure 6. The ortho protons were not included in the linear least-squares fit, as the geometric factors for these protons are especially sensitive to geometry (rotation of the phenyls and position of the iron with respect to the N$_4$ plane) and some direct contact contribution is possible. The slopes of the two plots are similar (−0.20 in Figure 6a and −0.24 in Figure 6b). From the dipolar analysis of the shifts, the magnetic anisotropy, $\chi_{\parallel} - \chi_{\perp}$, is calculated to be −357 × 10^{-6} cgsu. The solution magnetic moment measured for both BuNH$_2$ complexes is 2.9(1) μ_B per dimer consistent with an S = 1 ground state.[15] This leads to calculated g values of $g_{\perp} =$ 2.09, $g_{\parallel} = 1.98$. A small **g** tensor anisotropy is also found in the rhombic EPR spectrum of low spin monomeric Fe((DMG)-BF$_2$)Cl$_2^-$ ($g_x = 2.341$, $g_y = 2.191$, $g_z = 1.962$)[1b] (the μ-oxo species are EPR silent). The g values are significantly different for a low-spin heme imidazole complex ($g_x = 2.29$, $g_y = 1.57$,
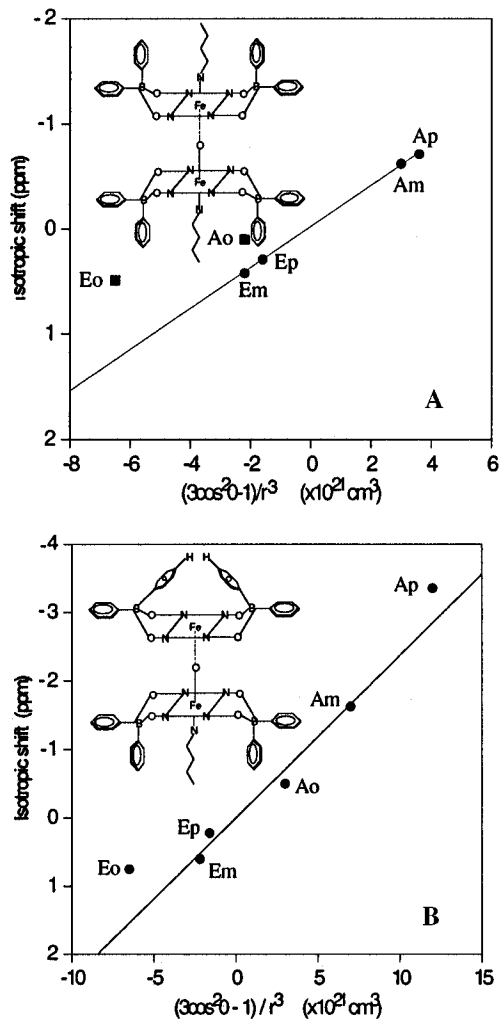

Figure 6. Plots of the isotropic shifts for the BPh$_2$ phenyl protons vs calculated geometric factors based on the structures shown: (A) bis BuNH$_2$ complex; (B) mono BuNH$_2$ complex with the vacant binding cavity collapsed.

$g_z = 2.90$).[16] (In the axial approximation $g_{\perp} = 2.26$, $g_{\parallel} = 1.962$ for the former and $g_{\perp} = 1.96$, $g_{\parallel} = 2.9$ for the latter.) The sign of $\chi_{\parallel} - \chi_{\perp}$ for the μ-oxo complexes is the same as that found for the monomeric dichloro complex and opposite to that for Fe(porphyrin)(IM)$_2^+$. Thus dipolar shifts for the ligated μ-oxo complexes are in the opposite direction and about one-fourth the magnitude of those reported by La Mar[12] for low-spin FeTPP(IM)$_2^+$ complexes.

The metal−metal-bonded [RuTPP]$_2$ dimer is somewhat analogous to our μ-oxo species. It is low spin ($\mu = 2.8$ μ_B, $\chi_{\parallel} - \chi_{\perp} = -1120 \times 10^{-6}$ cgsu) and also has two unpaired electrons in an orbital with π symmetry.[14]

Contact Shifts. DMG Methyls. The shifts for the DMG methyls of the various ligated μ-oxo species are collected in Table 5. The dipolar contribution is estimated as +2 ppm and is not expected to differ significantly in the various species. Contact shifts for the DMG methyls differ from the observed shifts in Table 5 only by a constant additive factor of −4.7 ppm.

The shifts are consistent with the effects of π spin transfer from a d$_{yz}$ orbital of the low-spin Fe to DMG π orbitals.[12] Variations of the methyl contact shifts with the nature of the trans ligand reflect subtle differences in spin density. These differences may be related in part to differences in the position

(13) More complicated models[14] were considered, but the simplest, which assumes the contribution from the nearest Fe is dominant, is considered adequate in this case.

(14) Collman, J. P.; Barnes, C. E.; Swepston, P. N.; Ibers, J. A. *J. Am. Chem. Soc.* **1984**, *106*, 3500−3510.

(15) Isotropic shifts for the bis 1-MeIM complex of **1** were found to obey the Curie−Weiss law over the temperature range 233−333 K, consistent with the existence of a single S = 1 spin state for this complex over this temperature range.

(16) Tang, S. C.; Koch, S.; Papaefthymiou, G. C.; Foner, S.; Frankel, R. B.; Ibers, J. A.; Holm, R. H. *J. Am. Chem. Soc.* **1976**, *98*, 2414.

Table 7. Geometric Factors and Shift Analysis for Axial Ligand Protons

L	position	$(\Delta H/H)_{iso}$[a]	G[b]	$(\Delta H/H)_{dip}$	$(\Delta H/H)_{con}$	FeTPP[c]
		BPh$_2$				
		LFeOFe				
1-MeIM	1-Me	−6.2	+8.0	−1.6	−4.6	+10.3
	2-H	+15.3	+21.6	−4.3	+19.6	−28
	4-H	+7.5	+20.9	−4.1	+11.6	−8.2
	5-H	+8.3	+13.4	−2.6	+11.0	−7.6
5-MeIM	1-H	+5.0	+13.5	−2.7	+7.6	−9.6
	2-H	+19.2	+21.6	−4.3	+23.5	−28
	4-H	+12.7	+20.9	−4.1	+16.8	−8.2
	5-Me	−3.0	+7.5	−1.5	−1.5	+9.0
1,2-Me$_2$IM	1-Me	−5.4	+8.0	−1.6	−3.8	+10.3
	2-Me	−17.1	<+0.2	<−0.04	−17.1	+12
	4-H	+6.8	+20.9	−4.1	+11.0	−8.2
	5-H	+9.6	+13.4	−2.7	+12.2	−7.6
4-Me$_2$N(PY)	2-H	+23.0	+22.0	-4.4	+27.4	
	3-H	+4.0	+12.0	−2.4	+6.4	
	4-Me	−9.1	+4.0	−0.79	−8.3	
		LFeOFeL				
1-MeIM	1-Me	4.3	+8.0	−1.6	5.9	+10.3
	5-H	−11.2	+13.4	−2.6	−8.6	−7.6
BuNH$_2$[d]	β	−2.36	+18.2	−3.6	1.3	
	γ	−0.61	+6.5	−1.3	0.7	
	δ	−1.22	+5	−1	∼0	
		BF$_2$				
		LFeOFeA				
1-MeIM	1-Me	+6.1	+8.0	−1.6	+7.7	+10.3
5-MeIM	5-Me	+1.8	+7.5	−1.5	+3.3	+9.0
1,2-Me$_2$IM	1-Me	+5.1	+8.0	−1.6	+6.7	+10.3
	2-Me	+16.6	+0.2	−0.04	+16.7	+12.0
		LFeOFeL				
1-MeIM	1-Me	+6.0	+8.0	−1.6	+7.6	+10.3
	5-H	−10.4	+13.4	−2.6	−7.8	−7.6
5-MeIM	1-H	−10.1	+13.5	−2.7	−7.4	−9.6
	2-H	−29	+21.6	−4.3	−24.7	−28.0
	4-H	−13.0	+20.9	−4.1	−8.9	−8.2
	5-Me	+1.5	+7.5	−1.5	3.0	+9.0
4-Me$_2$N(PY)	2-H	−23.5	+22.0	−4.4	−19.1	
	3-H	−8.4	+12.0	−2.4	−6.0	
	4-Me	+10.7	+4.0	−0.79	+11.6	

[a] Isotropic shifts in ppm using diamagnetic positions based on a related Fe(II) complex[7a] where available or for free ligand otherwise. Positive shifts are downfield. [b] Calculated from relevant structural data[1a,7d] or from ref 12b. [c] Contact shifts reported for the monomeric low-spin imidazole heme complexes from ref 12a. [d] Diamagnetic positions are based on the sandwiched BuNH$_2$ in Fe((DMG)BPh$_2$)$_2$-(PMePh$_2$)(BuNH$_2$): α-CH$_2$ 0.266, β-CH$_2$ −0.10, γ-CH$_2$ 0.39, δ-CH$_3$ 0.40 ppm.

of the iron with respect to the N$_4$ plane. Overlap between d$_{yz}$ and the oxime π orbitals and presumably the transfer of spin improve as the iron moves into the N$_4$ plane. X-ray structural data show[1a] that the strong trans BuNH$_2$ ligand pulls the iron almost into the N$_4$ plane. Weaker and sterically less demanding nitrile ligands may leave the iron out of the N$_4$ plane toward the oxo group while those with significant contacts with the N$_4$ plane may have the iron displaced to the distal side. The trends in the DMG methyl shifts in the (CH$_3$CN)Fe−O−FeL species in Table 5 may be related to these considerations. The greatest asymmetry is found for pyridine and 1,2-Me$_2$IM ligands, ligands which show the greatest reduction in K_2 in the BPh$_2$ system.

Axial Ligand Shifts. An analysis of the shifts for some of the axial ligands in terms of dipolar and contact contributions is given in Table 7. Some contact shifts for imidazoles in low-

(17) (a) Banci, L.; Bertini, I.; Luchinat, C. *Struct. Bonding* **1990**, *72*, 113−136. (b) Kollmar, C.; Couty, M.; Kahn, O. *J. Am. Chem. Soc.* **1991**, *113*, 7994−8005.

spin monomeric hemes derived by La Mar are included to illustrate a rough correspondence between these systems. We assume a single-ligated geometry for all species and ignore contributions from the remote iron in evaluating the dipolar shifts, as was done for the BPh$_2$ protons above. Diamagnetic positions are based on Fe(II) complexes where available or those of the free ligand if not. The precise values for contact and dipolar shifts depend somewhat on these assumptions. The essential features, however, are unlikely to depend on such details.

Only the more distant protons of the butylamine ligand were located (β, γ, and δ). In this case we used the Fe(II) complex Fe((DMG)BPh$_2$)$_2$(PMePh$_2$)(BuNH$_2$), which best simulates the sandwiched geometry of the BuNH$_2$ ligand, to estimate the diamagnetic positions. The shifts primarily reflect dipolar effects. Contact contributions are expected and found to be small for a σ donor attached to a metal with spin in a π orbital.

For the pyridine and imidazole ligands, direct transfer of spin from d$_{yz}$ to π orbitals of the ligand produces significant contact contributions to the shifts. The pattern of contact shifts is fully consistent with a π-delocalization mechanism which produces ^{1}H NMR shifts of opposite sign for ring protons and ring methyls. In the monoligated species negative π-spin density is introduced into the axial heterocycles, producing contact shifts in the opposite direction compared to those found in the fully ligated species. The fully ligated species (LFe−O−FeL, LFe−O−Fe(CH$_3$CN)) give contact shifts for axial ligands not unlike those found in monomeric hemes involving a similar spin-delocalization mechanism.

There is no precedent for axial ligand contact shifts in μ-oxo systems let alone for the negative spin densities found in the monoligated complexes. The theoretical principles necessary for understanding the NMR parameters in magnetically coupled dimers are complex,[17] and only a qualitative explanation can be offered at this point.

The π MO's containing the two unpaired electrons in the monoligated species are nondegenerate and delocalized over both irons with a node at the oxo atom. The amount of Fe$_U$ and Fe$_L$ character (U = unligated, L = the ligated iron) in each MO will differ as will the mixing with DMG and axial ligand π orbitals. The net spin density felt by a given proton will be the sum of the contributions from the two unpaired electrons. The negative spin densities found in the monoligated species may be a consequence of the spin transfer from the remote iron (as it passes through a node) or may be related to some correlation between the two spins. The DMG methyl shifts in the monoligated complex probably reflect a similar phenomenon. Those on the unligated half are primarily dipolar and downfield, while those on the ligated half are primarily contact and upfield.

Conclusions. Strong-field N$_4$ ligands such as bis(dioximes) lead to low-spin μ-oxo complexes which bind ligands trans to the oxo bridge. The BPh$_2$ superstructure modifies the binding energetics directly through nonbonded contacts with the ligand and remotely via peripheral contacts transmitted to the second site. Distinctive patterns of paramagnetic shifts are elucidated for the first time in the various ligated forms of low-spin d^5 μ-oxo complexes.